Faculty and Researchers | Faculty and Researchers' Publications

2021

High-stability tin/carbon battery electrodes produced using reduction expansion synthesis

Lee, Tongli Lim; Adams, Ryan A.; Luhrs, Claudia; Arora, Anjela; Pol, Vilas G.; Wu, Chun-Hsien; Phillips, Jonathan

http://hdl.handle.net/10945/68921

High-stability tin/carbon battery electrodes produced using reduction expansion synthesis

Tongli Lim Lee [a], Ryan A. Adams [b], Claudia Luhrs [a], Anjela Arora [b], Vilas G. Pol [b], Chun-Hsien Wu [a], Jonathan Phillips [c, *]

[a] Mechanical and Aerospace Engineering, Naval Postgraduate School, 833 Dyer Rd., Monterey, CA 93943, USA
[b] Davidson School of Chemical Engineering, Purdue University, 480 Stadium Mall Dr., West Lafayette, IN 47907, USA
[c] Energy Academic Group, Naval Postgraduate School, 1 University Dr., Monterey, CA 93943, USA

ARTICLE INFO

ABSTRACT

This study shows high stability Sn (10 wt %)/carbon Li-ion battery anodes can be made via the Reduction Expansion Synthesis (RES) process. Hybrid Sn/C anodes had an initial capacity of 425 mAh g-1 which stabilized to ~340 mAh g-1 after less than 10 cycles. Unlike earlier Sn/C anodes, capacity remained virtually constant for more than 180 additional cycles. Neat carbon independently tested for Li capacity had a steady specific capacity of 280 mAh g-1. The difference detected between the pure carbon and Sn/C cases are consistent with Sn having the theoretical capacity of ~1000 mAh g-1. The high stability of the RES derived anodes, relative to earlier Sn based electrodes, is postulated to exist because RES synthesis enables the formation of direct, strong bond between Sn and carbon substrate atoms, hence reducing the rate of Sn electrode disintegration and capacity fade due to expansion upon lithiation. X-ray diffraction and transmission electron microscopy are consistent with this postulate as both show an initial Sn particles size of only a few nanometers and minimal growth after cycling. Reduced interface resistance is also indicative of unique Sn-carbon bond.

Published by Elsevier Ltd.

1. Introduction

There is considerable effort to increase the net energy density of rechargeable lithium ion batteries by developing anodes with higher capacities than graphite. One of the difficulties with increasing the anode capacity is that many of the conductive structures, other than graphite, tend to pulverize after lithium incorporation, leading to significant capacity loss after only a few charge/discharge cycles. Much effort in this field has been focused on creating conductive metal oxide/graphene composites, structured in such a fashion that the metal oxides are physically prevented from crumbling [1,2]. For example, there are many studies focused on Fe_3O_4 mixed/fixed on different conductive forms of carbon because iron oxide not only has a potentially high maximum capacity, 922 mAh g^{-1} [3], but also meets conductivity, cost and environmental objectives. This is far higher than that of the graphite electrode, 372 mAh g^{-1} [4], due to the final Stage 1

structuring Li/C stoichiometry of LiC_6 [5,6]. Another material, with an even higher theoretical capacity, lower operating potential than metal oxides for enhanced full cell energy density, and decreased voltage hysteresis due to the alloying storage mechanism, is metallic Sn. The final stoichiometry of Li/Sn, $Li_{22}Sn_5$ has a high lithium packing density (75.47 mol L^{-1}), which is nearly as high as that of pure lithium metal (76.36 mol L^{-1}) [5,7]. This packing density yields a theoretical capacity of 990 mAh g^{-1} for Sn. However; like the other alternatives to graphite, Sn is not employed because of mechanical pulverization which leads to rapid deterioration of capacity over extended cycling. In particular, Sn expands so significantly (~360%) during lithiation, and then shrinks during discharging, that it physically pulverizes during cycling, creating an unstable and unusable electrode. Specifically, disintegration leads to a rapid drop in capacity with cycling and excessive solid electrolyte interphase (SEI) formation, rapidly consuming electrolyte and increasing electrode resistance [8]. As with magnetite, novel approaches to mitigate the crumbling that accompanies expansion during lithiation have been tried. For example, the encapsulation of Sn within nano-scale conductive carbon structures, with void space to accommodate expansion without concomitant breakage [9–12],

yields high, ~600 mAh g^{-1} [12] and sometimes very high, ~1500 mAh g^{-1} [9] initial capacity, and improved, but still not sufficient, cycling stability. For example, despite the impregnation of Sn nanoparticles within amorphous carbon nanotubes as a structural support and conductive pathway, the capacity fades by 29% over the first 100 cycles (0.2 A g^{-1}) to 720 mAh g^{-1}, demonstrating the need for increased stability in Sn/C composite anode materials [13].

The present study is based on the hypothesis that a novel synthesis method, called Reduction Expansion Synthesis (RES), can successfully produce stable Sn/carbon composite anodes for Li-ion batteries. The novelty of RES is that reducing species are introduced to a synthesis not as a gas (e.g. CO, H$_2$), but rather as the radicals generated by the *in situ* thermal decomposition of a solid. Graphene [14,15], supported metal catalysts [16], small iron and nickel particles [17], and alloys of the same [18–20], have all been synthesized employing variations on RES batch processing. In all cases, the thermal decomposition of urea was used to generate radicals that promote the reduction of the reactants.

The products of RES have shown superior properties in some respects to those synthesized using standard techniques. For example, iron and nickel particles produced by the simple RES process at only 800 °C, are about 1 μm average size, far smaller than those made using the standard industrial techniques, such as atomization at ~1500 °C [21] or grinding [22]. More germane to the present study is the remarkable sintering resistance of supported metal catalysts particles synthesized using RES. They were found to be smaller and more stable in a fuel cell than metal catalysts prepared by incipient wetness. Given the morphological similarity between a composite Sn/C electrode and a supported metal catalyst, the unusual stability of RES generated metal catalysts suggested similar properties for Sn/C produced by RES, leading to a Sn based, high capacity, stable, Li battery electrode.

The results, in brief are that the Sn/C anodes generated using RES have a significantly higher capacity than pure carbon electrodes for Li ions, and are far more stable during lithiation than traditionally prepared Sn containing anodes. It is also clear that as the synthesis process is very rapid (ca. 100 s), and the materials used are standard and inexpensive, the RES process may have economic advantages over other anode synthetic approaches that require expensive/exotic materials. Although the tests conducted are specific to Sn, the data are consistent with the postulate that other metals, such as those capable of intercalating Na ions, can be produced as small, stable particles on relatively inexpensive forms of carbon.

2. Experimental

2.1. Electrode production protocol

Sn/C battery electrodes were created using the simple process outlined below, which is a variation on the RES process employed to make supported metal catalysts, as described in prior literature [16]. The primary novelties of this synthesis were the use of a carbon support, and the inclusion of an activation step (STEP I), intended to create oxygen groups on the carbon substrate prior to the addition of the Sn and urea.

STEP I. A commercial high surface area carbon (Vulcan XC 72, from Cabot, Corp.) was 'activated'. Specifically, a bed of carbon powder less than 2 mm deep was heated in air to 600 °C for 10 min in a tube furnace. This process reduced the weight of the carbon by approximately 11% and, as described in the scientific literature [23–26], introduces many oxygen species on the surface of the carbon via the partial combustion of the carbon.

High surface area carbon partially burned in oxygen, hence covered in oxygen species chemically bonded to carbon in the surface, is generally referred to as 'activated carbon'.

STEP II. Sn(II) chloride, urea, and water, were mixed in the weight ratio of 1: 1: 20. The final mix, herein 'Sn/urea' is a homogeneous paste containing dissolved species.

STEP III. The materials produced in Steps I and II were mixed in weight ratio of 1 activated carbon: 8.8 Sn/urea. The mixing was done in a mortar and pestle, by hand, and the final material (Fig. 1) had the consistency of a wet paste.

Step IV. The paste was then placed in 20 cm^3 volume alumina boat, and the boat inserted into a quartz tube approximately 75 cm long and ~2.5 cm O.D. The tube was placed in a standard laboratory 45 cm long tube furnace, and attached via standard gas plumbing fixtures, to a gas supply system to allow control of gas identity and flow rate through the tube.

Step V. The quartz tube was arranged such that the alumina boat was in the center of the furnace, and then 99.99% N$_2$ gas was passed through the tube at ~100 sccm, via a rotameter. Concomitantly the furnace was brought to a temperature of 100 °C for an hour to remove excess water from the sample.

Step VI. Two changes were made. First the gas flow rate was reduced to 5 sccm. Second the furnace temperature was increased to 800 °C. The furnace took approximately 4 min to reach 800 °C. Once that temperature was achieved it was only maintained for an additional 30 s.

Step VII. Immediately upon the completion of Step VI, the quartz tube containing the sample was removed from the furnace, and placed on a rack to cool. The nitrogen gas flow rate during cooling was increased to 100 sccm.

In addition to making a Sn/C electrode employing the RES protocol outlined above, a control sample was created in which no activation step was included. That is, the process employed was identical to the one given above, except Step I was not conducted. It was postulated that in this case few, if any, surface radicals would be produced on the carbon during the remaining RES steps, hence there would be no mechanism for direct chemical interaction between carbon and Sn. This would lead to the formation of large (ca. micron) Sn particle formation. Additionally, a sample was prepared involving everything but addition of Sn(II) chloride, which will be XC-72 neat carbon (0% Sn/C composite). Other controls, such as never introducing urea are possible, but the entire literature on Sn/
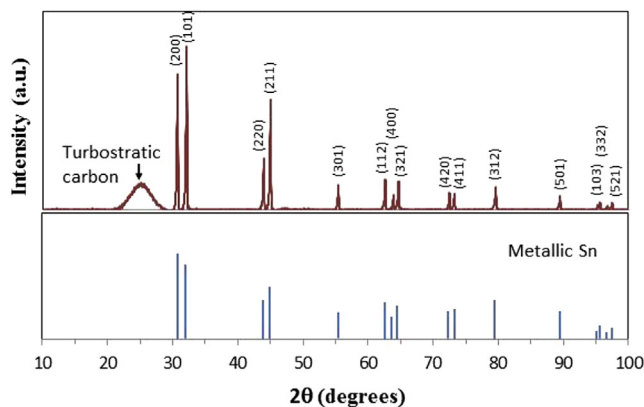

Fig. 1. *XRD of Sn/C Powder Before Cycling.* The dominant phase of the Sn is clearly metallic tetragonal Sn. The broad peak at ~25° 2theta originates from the carbon substrate. Using the Debye-Scherrer equation ((200) peak) the average Sn particle size was determined to be ~15 nm before cycling and ~20 nm after cycling. (A colour version of this figure can be viewed online.)

Carbon is a 'urea free' control. The conclusion: Stable tin particles are never produced on carbon in any process in which urea is absent.

2.2. Analytical instruments

Three instruments, located at the Naval Postgraduate School in Monterey, CA were employed in the analysis of the morphology of the Sn/C electrode: transmission electron microscopy (TEM), scanning electron microscopy (SEM) and x-ray diffraction (XRD). The TEM is a Tecnai Osiris, a fully digital 200 kV S/TEM system, as well as technology for EDX signal detection/mapping at the 0.1 nm level. The SEM is a Zeiss Neon 40 with a resolution of 1.1 nm. The XRD is an Rigaku MiniFlex, a general purpose X-ray powder diffractometer, with Cu tube and PDXL, Rigaku's full-function powder diffraction analysis package. Image J and JMP were employed for image/data analysis.

Raman spectra were collected with a Thermo Scientific DXR Raman Microscope using a 632 nm laser at 2 mW power at Purdue University. Elemental analysis of prepared samples was determined using an Exeter Analytical CE440 CHN/O/S instrument at Purdue University.

2.3. Half-cell testing

Electrochemical Characterization: To electrochemically test the Sn/C composite material, laminates were constructed at Purdue University by taking a ratio of 80 wt % active material, 10 wt % carbon conductive additive (Timcal Super C65), and 10% wt. % binder (sodium carboxymethyl cellulose). A slurry was formed utilizing ultrapure water as solvent and mixed for 20 min before coating onto a copper foil. After drying for 12 h in a vacuum oven set to 80 °C, electrodes with a diameter of 12 mm were punched out (active material loading of ~1.5 mg cm^{-2}). Coin cells (2032 type) were assembled in an Argon atmosphere (99.998%) high purity glovebox. For Li-ion half cells, lithium metal foil was used as the counter electrode, with 1.0 M LiPF$_6$ in ethylene carbonate/diethyl carbonate/dimethyl carbonate +3% fluoroethylene carbonate additive as electrolyte and Celgard 2500 as separator. Cyclic voltammetry was performed at a scanning rate of 0.1 mV s^{-1} utilizing a Gamry 600 + instrument. Potentiostatic electrochemical impedance spectroscopy (EIS) was collected on fresh cells and after 10, 20, and 50 cycles at 1.25 V vs. Li$^+$/Li in a frequency range of 0.01—10^6 Hz utilizing a Gamry 600 + instrument. All galvanostatic cycling was conducted with an Arbin cycler, with current densities ranging from 20 to 500 mA g^{-1} in a voltage range of 0.005—1.5 V vs. Li$^+$/Li. For post cycled electrode material analysis, coin cells were opened in the Argon glovebox and washed with DMC and vacuum dried to remove electrolyte and salts.

3. Results

3.1. Morphology

The purpose of the morphological analysis was to determine the form and structure of the Sn particles, and to contrast the particle size observed before and after cyclic electrochemical testing. Moreover; particle size measurement serves as a test of the hypothesis that the RES synthesis creates metallic Sn particles bonded directly to carbon atoms in the surface. Small particles (ca. <20 nm) are consistent with the hypothesis, whereas large particles (>1 μm) clearly indicate little or no interaction between carbon and Sn, hence the rapid sintering generally associated with the use of carbon as a support for heterogeneous catalysts.

The XRD studies of the 10% Sn/C sample prepared using the standard RES protocol clearly showed that virtually all the Sn was present as metallic Sn both before (Fig. 1), and after electrochemical cycling. In contrast, the control sample was found to be primarily Sn-oxide and ~20% metallic Sn. Moreover, line broadening, using Debye-Scherrer analysis, suggested the average particle size was about 15 nm for the former. The particle sizes determined using the Debye-Scherrer approach are larger than the apparent size from TEM imaging (below), but as discussed in detail later, this difference is anticipated as the relative weighting of large and small particles is significantly different in the two methods [27—30]. Consistent with the observations in the present work, the half-height Debye-Scherrer method generally yields an 'average' particle size larger than that obtained from TEM analysis. In this case, as will be later shown, the TEM analysis showed a much smaller mean particle size, but both methods indicated little sintering during lithiation.

Control studies were undertaken to determine if small particles would form on carbon surfaces not properly prepared to create Sn-carbon bonding sites. In the principle control study the carbon was not 'activated'. All the steps in the protocol described in the experimental section were carried out identically except for Step 1. Step 1 was modified; the carbon was heated in flowing nitrogen gas (99.99%), rather than air, to 600 °C. Furthermore, the carbon as received was found to be hydrophobic based on the simple test: A drop of water placed on top of the carbon did not wet the sample. The water drop simply broke up into smaller drops, each more than 10 μm across and easily visible to the unaided eye. Hence, the carbon initially had few if any surface oxygen groups [26] fresh out of the bottle, and given no air/oxygen 'activation' pretreatment, no oxygen should be found on the surface if Step 1 is not employed. Notably, a drop of water placed on the same carbon after proper activation, using the unmodified Step I protocol, completely disappears. The water clearly wets the material, leading to the conclusion that activation creates oxygen groups that act as primary adsorption sites.

To verify the proposed Step I air activation and targeted 10% Sn/C weight loading, elemental analysis was performed for the XC-72 neat carbon and 10% Sn/C composite as shown in Table 1. To obtain the value for Sn, the percentages were subtracted from 100%, with standard errors reported and all reported values in terms of weight percentage. Noticeably, the air activation does increase the amount of oxygen functionalities, as pristine Vulcan XC-72 is specified to be >99% carbon. The targeted value of Sn loading is achieved, signifying the successful incorporation and mixing of the Sn (II) chloride precursor onto the carbon substrate.

Raman spectra were collected for the XC-72 neat carbon and 10% Sn/C composite produced by RES process as shown in Fig. 2. Two primary peaks are observed at 1320 cm^{-1} at 1580 cm^{-1} correlating to disordered carbon (sp^3) and graphitic carbon (sp^2), respectively. The ratio (I$_D$/I$_G$) of these peaks is ~1.3 for both samples, indicating the high disordered nature of this carbon, and that the carbon structuring is unaltered by the RES process. No additional peaks are observed in the 10% Sn/C composite, which agrees with the XRD results showing no Sn oxide phase formation, as metallic Sn will not be Raman active.

Are control studies needed? It is notable that in many studies of anodes composed of multiple materials, no independent studies of

Table 1
Elemental analysis of prepared XC-72 neat and 10% Sn/C composite materials by RES process.

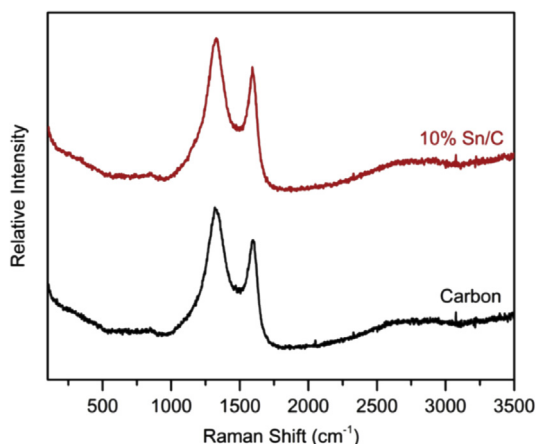| Sample	C	H	N	O	Sn
XC-72 neat	95.05 ± 0.41	0.81 ± 0.04	0.16 ± 0.03	3.91 ± 0.48	—
10% Sn/C	84.77 ± 0.57	0.89 ± 0.03	0.40 ± 0.04	3.58 ± 0.56	10.35

Fig. 2. *Raman Spectra.* Top: 10% Sn/C. Bottom: XC-72 neat carbon. Raman spectra collected with a 632 nm laser at 2 mW power. (A colour version of this figure can be viewed online.)

Fig. 4. TEM/HAADF STEM Mode Images of Standard Protocol Sn/C. A) Sample before cycling, 50 nm scale, B) Sample before cycling, 20 nm scale, C) Sample after cycling, 20 nm scale, D) Elemental map of Sn corresponding to (B). (A colour version of this figure can be viewed online.)

the conductive 'support' are included, even though in general the weight fraction of the support is greater than 30% [2]. Thus, studies that neglect consideration of the support contribution may imply an overstatement of the role of the purported 'active phase', e.g. magnetite. A good example is graphene, a common element in many 'conductive oxide' based electrodes, because it has clearly been experimentally demonstrated that neat graphene has a capacity between 500 and 800 mAh g^{-1} by itself [3].

The morphology of particles formed in the principle control study indicates the need for carbon activation to create highly dispersed Sn particles using the RES process. As shown in Fig. 3, multi-micron, spherical particles form on the surface of carbon which was not activated. XRD studies reveal these particles are a mix of Sn oxide and metallic Sn. This is consistent with the case of minimal bonding between the carbon surface and the tin. The carbon surface is effectively 'Tin phobic'. Upon heating, the tin rapidly diffuses across the surface, leading to agglomeration and the formation of particles millions of times larger, by volume, than those found to form on activated carbon as described below.

Both SEM and TEM were employed to the study of particles formed by the RES method on activated carbon. Although XRD (Fig. 1) and chemical analysis clearly showed significant Sn on the carbon, a thorough SEM investigation revealed no apparent Sn structures. This is consistent with all Sn structures being too small and highly dispersed for easy observation using SEM, although EDS analysis in the SEM corroborated the Sn presence. Moreover, given the high temperature encountered, 800 °C, it suggests that the Sn
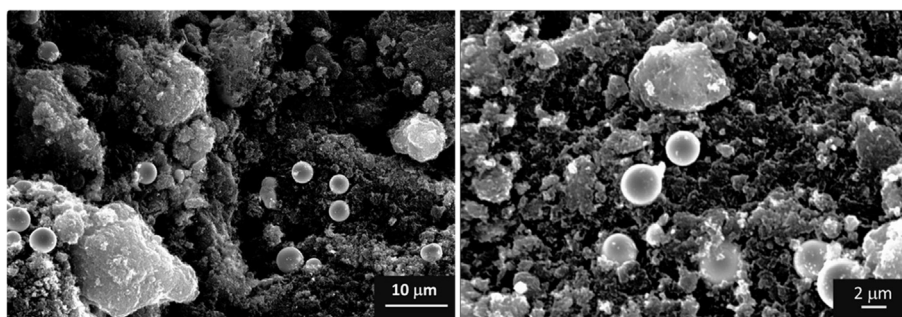
metal is strongly bonded to the carbon surface. Only strongly bonded metal by carbon would resist sintering at 800 °C, as described in the reaction mechanism in the discussion section.

HAADF STEM analysis (Fig. 4) was consistent with the XRD, and SEM, indicating that only very small Sn particles were present on the carbon surface. None of the particles before battery testing appear to be larger than 5 nm (Fig. 4A and B). The images show after more than 100 full charge-discharge cycles there is some level of particle sintering. Some particles are 'large' of the order 10 nm across, but the majority are still less than 5 nm in size. Still, there is no evidence of 'pulverization'. Thus, qualitatively the XRD and the TEM results are consistent, leaving little doubt that very small metallic Sn particles form following the standard RES protocol, and that limited growth occurs during cyclic electrochemical testing.

The particle size distributions were measured from the TEM images. Software Image J was employed to measure the particles and JMP to generate the histograms and perform the statistical analysis. A mean value close to 2 μm was obtained for the sample as prepared by RES approach when the carbon was activated, while a

Fig. 3. *Sn Particle Size on non-Activated Carbon.* - The dominant Sn structure found to form on non-activated carbon were large (ca. ~2 μm) particles, that XRD and EDX showed to be mostly Sn oxide. Sn particles are the bright spherical particles seen in the figures (left: 10 μm scale and right: 2 μm scale). Using SEM, no particles could be detected on similarly Sn loaded activated carbon [31].
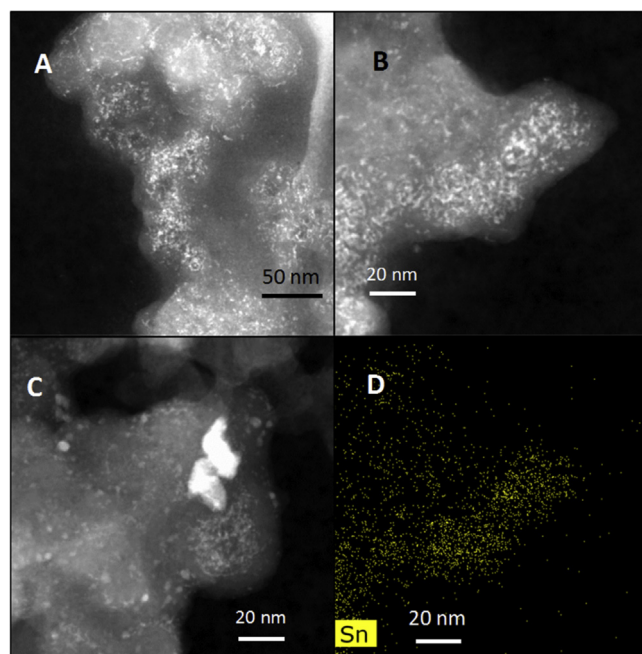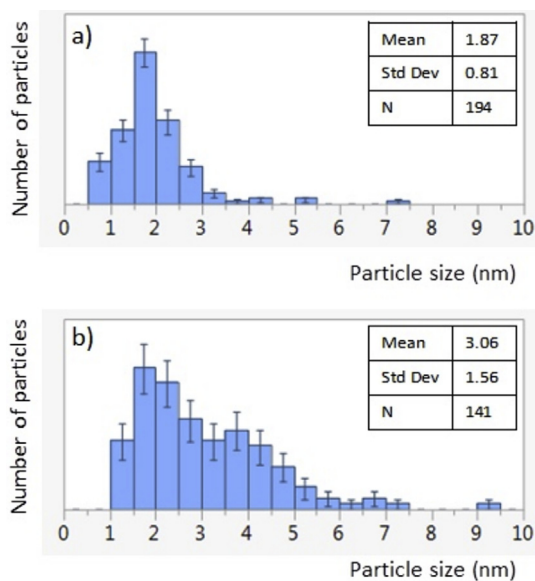
Fig. 5. Particle size distributions generated from the STEM/HAADF images before (a) and after (b) cycling. (A colour version of this figure can be viewed online.)

mean of 3 nm was observed for post-cycled specimens (Fig. 5). It is worth noting that although the before and after cycling particle size values are very close, the post-cycled sample does show a tail in the PSD that extends to 10 nm. These values are much smaller than the those calculated from XRD FWHM analysis.

3.2. Electrochemical analysis

The 10% Sn/C electrode was tested in a Li-ion half-cell for electrochemical performance as shown in Fig. 6. Formation cycles were analyzed using cyclic voltammetry (Fig. 6a), where a few peaks are observed in the first discharge at 0.9 V, 0.45 V, 0.3 V, and 0 V, likely due to initial SEI formation, Sn alloying with Li, and intercalation into the carbon support respectively. Subsequent cycles show fewer features, with a charge peak at 0.7 V but otherwise smooth profile due to the high percentage of amorphous carbon in the composite. Galvanostatic cycling test at constant current is shown in Fig. 6b, and a stable composite capacity of 350 mAh g^{-1} at 50 mA g^{-1} is achieved after capacity loss in the first 10 formation cycles. Cycling at various current densities is shown in Fig. 5c, with the corresponding charge-discharge voltage curves in Fig. 5d. From a capacity of 370 mAh g^{-1} at 20 mA g^{-1} to 220 mAh g^{-1} at 500 mA g^{-1}, this material demonstrates exceptional rate kinetics as compared to graphite, due to the high surface area carbon and small Sn particle size enabling rapid lithiation/de-lithiation. The charge-discharge voltage profiles for the first two cycles are shown in Fig. S1. While there is a large first cycle capacity loss of 60% over the first few cycles, likely due to SEI formation on the high surface area carbon, the subsequent 140 cycles show great stabilization and coulombic efficiency.

To evaluate the contribution of the two components of the electrode, carbon and Sn, a control study was performed on the XC-72 carbon-neat. Although graphite has a theoretical capacity of 372 mAh g^{-1} for very slow discharge, it is not reasonable to presume a specific carbon with different structuring/material properties will be the same. Thus, a capacity measurement on the carbon
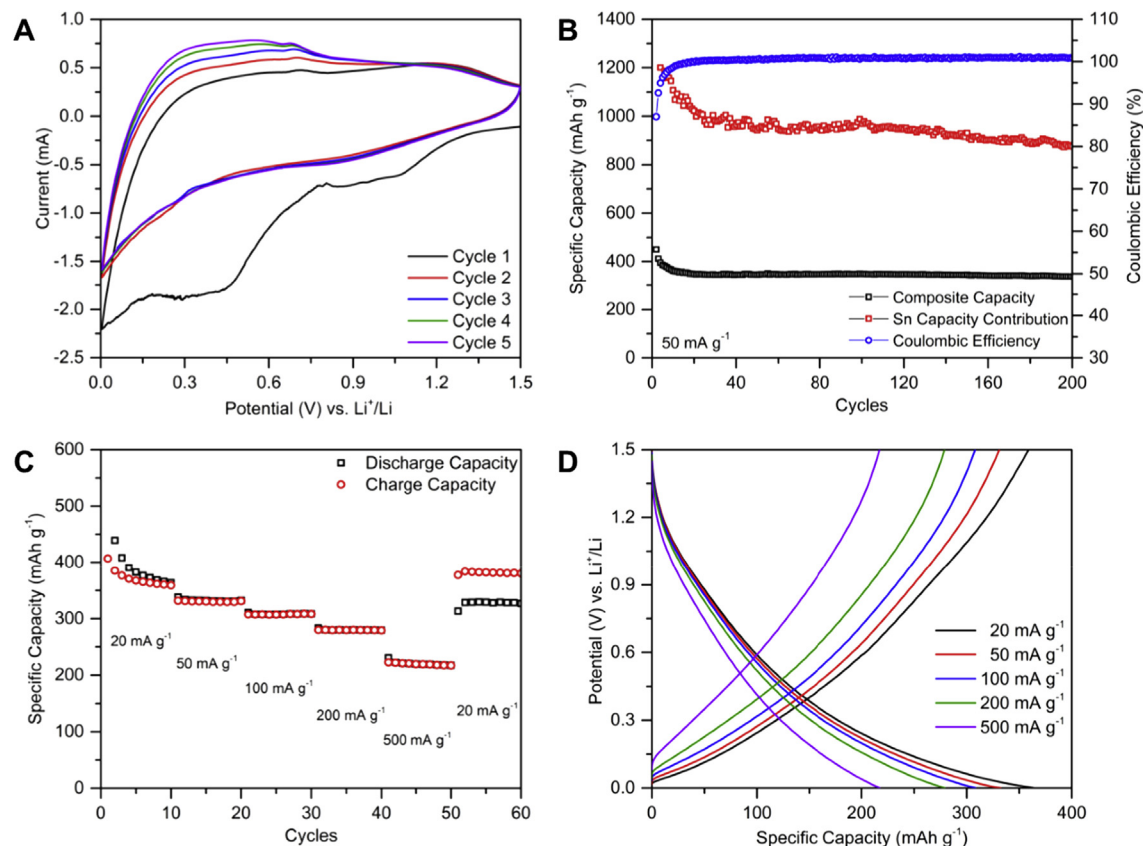

Fig. 6. *Electrochemical performance for 10% Sn/C anode material in Li-ion half cell.* (A) Cyclic voltammetry for first five cycles at 0.1 mV s^{-1} scan rate. (B) Long-term Galvanostatic cycling at 50 mA g^{-1} current density. (C) Galvanostatic cycling at various current densities (20–500 mA g^{-1}). (D) Stable charge-discharge voltage curves at corresponding current density from rate study. (A colour version of this figure can be viewed online.)

alone provides a value which can be subtracted from the measured capacity of the Sn/C electrode to determine the Sn contribution, with these calculated values shown in Fig. 6b. The carbon support showed a small drop over the first five cycles and then a stable capacity of approximately 280 mAh g^{-1} at a discharge rate of 50 mA/g. This confirms the specific capacity contribution from the nanosized tin particles, close to theoretical values of 1000 mAh g^{-1}, and the augmented rate capability at higher current densities.

The differential capacity (dQ/dV) was plotted for the 10% Sn/C and XC-72 carbon neat to see the differences in lithiation storage mechanisms over extended cycling, and is shown in Fig. 7. During cycle 1, the 10% Sn/C sample showcases additional peaks during discharge and charge associated with SEI formation and Sn alloying/de-alloying. It is interesting to note that after the first cycle, these additional peaks diminish in clarity, and that by cycle 50, the carbon and 10% Sn/C have similar profiles.

It is then interesting to see if the addition of Sn nanoparticles to the carbon support augments electrochemical properties of the material. Electrochemical impedance spectroscopy (EIS) was performed on both materials throughout cycling, to analyze the resistances introduced by charge-transfer mechanisms, SEI layer, and diffusional limitations, and is shown in Fig. 8. At open circuit voltage (Fig. 8a) before discharging, the SEI layer has not yet formed, and thus the semicircle in the high-medium frequency range can be attributed to charge transfer resistance. The addition of Sn nanoparticles clearly decreases charge transfer resistance by the smaller semicircle diameter and total material resistance. This is consistent with a strong bonding between Sn and C. The low frequency line can be modeled by a Warburg impedance, and reflects solid-state Li$^+$ diffusion, with similar profiles seen for both due to the similar carbon architecture. Through later cycles, even with the addition of SEI layer (at high frequency range), the 10% Sn/ C shows decreased charge-transfer resistance and overall material resistance as compared to XC-72 carbon neat, which can explain the augmented rate performance observed in the 10% Sn/C sample. The proposed morphology of small Sn nanoparticles well distributed and strongly attached to the activated carbon supports this dramatic improvement in overall electrode conductivity.

4. Discussion

This study was designed to test the postulate that RES synthesis of Sn/C electrodes can lead to strong bonding between metal and support leading to particle stability through charge/discharge and concomitant expansion/contraction of the Sn particles. This will lead to a capacity of the electrodes higher than that for the carbon support alone, a capacity for Li can be maintained over hundreds of charge/discharge cycles. This postulate rests on several prior observations and a model of carbon surface chemistry.

The most significant prior observation is that unique rafts, approximately 5 atoms each, formed during RES synthesis of Pt/ conductive substrate fuel cell electrodes [16]. The formation of these rafts on the underlying conductive substrate was postulated to result from a sequence of chemical processes: i) generation of free radicals via thermal decomposition of urea, ii) removal of surface oxygen atoms from the substrate by those reducing radicals consequently creating unsaturated surface sites, and iii) immediate bonding to these sites of Pt atoms released by thermal decomposition of platinum atom containing precursor molecules. The empirical outcome was consistent with this model. The RES synthesis clearly resulted in the creation of uniquely strong metal/ substrate bonds that prevented the type of Pt particle growth normally observed on fuel cell electrodes. Other observations of unique structures formed via RES synthesis are consistent with the general model of RES: thermal decomposition of urea releases
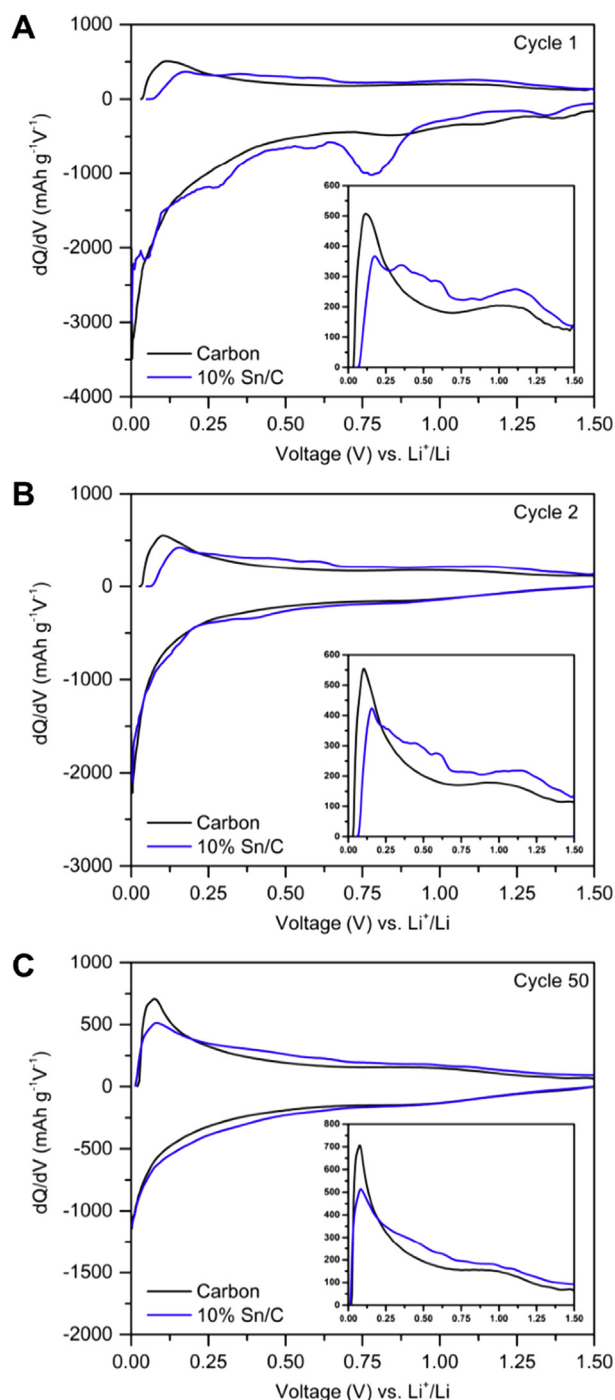

Fig. 7. Differential capacity curves for the 10% Sn/C by RES and XC-72 carbon neat electrodes to elucidate Li storage mechanisms. (A) Cycle 1. (B) Cycle 2. (C) Cycle 50. (A colour version of this figure can be viewed online.)

reducing radicals that permit unique chemical processes to occur. Unique RES syntheses consistent with the model include the reduction of graphite oxide to form graphene [14,15], and the reduction of metal oxide powders to yield sub-micron metal particles [17—20].

In order to explain more precisely the anticipated chemistry of RES generation of Sn/C electrodes it is necessary to present a condensed description of a widely accepted model of the creation of unsaturated, 'surface radical', sites on carbon [23—26]. Generally, carbon, either graphitic or turbostratic, surfaces consist primarily of
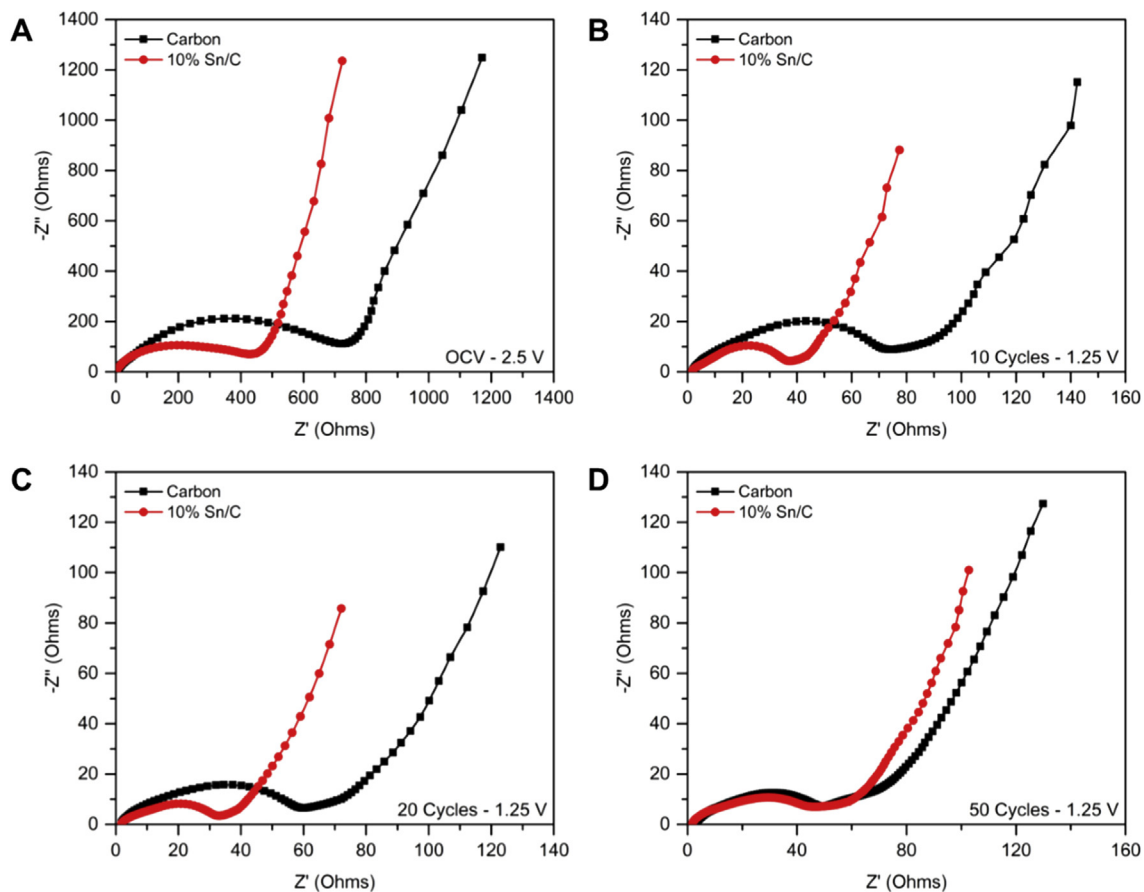
Fig. 8. Electrochemical impedance spectra for Li-ion half cells with either XC-72 neat carbon or 10% Sn/C by RES process. (A) OCV at 2.5 V. (B) After 10 cycles at 1.25 V. (C) After 20 cycles at 1.25 V. (D) After 50 cycles at 1.25 V. (A colour version of this figure can be viewed online.)

basal planes in which all atoms are strongly bonded to three nearest neighbors. Little chemistry takes place here. In contrast, at defect sites, including edges, there are surface sites capable of chemistry. In particular, O atoms, OH complexes, etc. often bond to unsaturated carbon atoms at these sites. It is well documented that O-groups, found at edges and defects, serve as the nucleation points for many processes including water adsorption [26], and metal particle formation [32,33], but not strong bonding. However; there are specific 'recipes' for removing O-species from these sites, such as heating to 950 °C in flowing inert gas, that remove C-atoms as well, and concomitantly create 'dangling bonds' or 'surface radicals'. The surface radicals so formed have been shown to form strong bonds to metal atoms [34–36].

To more fully understand the steps used in the RES synthesis, following is a brief review of recipes that remove oxygen from carbon surfaces, yet do not create surface radicals. For example, treating a carbon surface in hydrogen, at temperatures above 950 °C creates a hydrophobic, chemically inert carbon [26]. It is believed that the high temperature not only strips the oxygen groups from the surface, but also reacts with all 'surface radicals' created by the removal of oxygen to create methane. No highly reactive surface sites remain. One of the simplest tests of this postulate is a test of hydrophobicity. A carbon surface without oxygen groups or surface radicals is hydrophobic.

Returning to the hypothesis of this study: It is believed that during RES synthesis of the Sn/carbon electrodes two steps, previously only carried out sequentially [30], are combined into a single rapid synthesis. Specifically, during RES synthesis, reducing

radicals produced via urea decomposition attack oxygen groups on the carbon surface, leading to the formation of volatile, stable species. This process, Step I, creates carbon 'surface radicals'. Almost immediately these surface radicals form strong bonds with metal atoms, Step II. These metal atoms are generated via the decomposition of metal precursor molecules, a process that is thermally driven and takes place concomitantly with the thermal decomposition of the urea.

All the data collected in this study is consistent with the process outlined in the above paragraph. In particular these observations are consistent with this model: i) Very small Sn particles form. ii) The small Sn particles are stable even at 800 °C. iii) They sinter slowly during use as a Li ion electrode over hundreds of charge/discharge cycles and the accompanying expansion/contraction. iv) There is a reduction in the interface resistance of RES produced particles during charge/discharge. V) The same RES synthesis carried out on activated carbon (control study) does not produce highly dispersed Sn particles, but rather micron scale, spherical Sn particles. In this case no excess capacity is found. Also, different carbons used during RES synthesis may produce even greater stability.

Evidence for the various claims regarding particle size, stability in battery use, etc. are clearly found in the XRD, TEM and SEM data provided in the Results section. Indeed, the existence of very small Sn particles (<15 nm), even after the RES synthesis that involves a step at 800 °C, is found from XRD (Fig. 1), and TEM studies (Figs. 4 and 5). The data also shows that there is limited growth of the metal particles during battery testing. XRD spectra of 10% Sn/C

interpreted using the standard half-height Debye-Scherrer method indicates the average particle increases from ~15 nm to ~20 nm during testing. TEM images the particles directly, and it appears that the particles are smaller than predicted based on XRD. Indeed, initially no particles larger than 5 nm are observed, and the average appears to be significantly smaller than the one calculated from FWHM approach. After cycling particle sizes have a wider distribution, however still measure <10 nm. There is also indirect evidence of very small particles from SEM studies: no particles are observed, suggesting the particles are below the resolution size limit of the instrument.

One issue requiring added discussion is the difference in size of the Sn particles on the RES sample as determined by TEM and XRD. As noted earlier, the differences in size provided by these two methods has been reported repeatedly [27–30], hence it is unexceptional. Moreover, the difference is not germane to the primary thesis of this work. In fact, only the finding, by both methods, that the particles produced by the RES method are nanoscale and those generated on the control are micron scale, is relevant. To wit, particles prepared using RES are many orders of magnitude smaller by volume than those prepared in an identical fashion, but without the activation step (control). Given the process is a volumetric one, the volume ratio is the critical value. Even assuming the XRD provided size of the RES sample is accurate (~15 nm), and given that those produced on the control sample have an approximate average diameter of 3 μ (Fig. 3), by volume the particles on the control sample are 10 million times larger. Alternatively, assuming the TEM particle size is more accurate indicates the control sample particles are 100 million times larger by volume than those produced using the RES method. Both measurements are consistent with the central thesis of the model: RES produces stabilized, nanometer sized, particles.

After more than 150 charge-discharge cycles, as observed using TEM, most Sn particles are still less than 5 nm across, but some particles as large as 10 nm, form. This is remarkable for two reasons. First, in all prior studies in which Sn/C electrodes were synthesized and tested there was dramatic Sn particle growth, and/or Sn particle 'crumbling' after less than 20 cycles of anode testing [8,10,11,37]. Second, the standard methods for producing metal particles on carbon, even at weight loadings far less than that employed here, produce large particles that readily sinter [32,34,36].

Both the initial small size of the particles on the RES and the very slow sintering are consistent with one of the postulated requirements: for strong and direct chemical bonding and concomitant stabilization of nm scale particles: 'surface radicals' must form on the carbon. In the absence, initially, of a significant quantity of oxygen groups on the carbon, as testified by the hydrophobic character of the carbon, no surface radicals can be formed by removal of those groups by gas phase radicals. Notably, as summarized elsewhere [23,26], significant work shows that in the absence of surface oxygen groups carbon is hydrophobic. Hence, the 'control' sample had few if any oxygen groups, hence no oxygen could be removed during the heating step and concomitantly no surface radicals formed. In the absence of these radicals (e.g. control sample), bonding between and the carbon surface is very weak, leading to rapid sintering and concomitantly the formation of micron scale particles. In other words, urea alone is necessary but not sufficient to create direct Sn/C bonding. The surface must also be 'activated' before the urea/Sn precursor heating step, that is it must contain oxygen groups, such that surface radicals are generated by products of the urea decomposition. SEM was valuable in demonstrating the very different Sn particle growth process that occurs when not all the requirements for producing nano scale Sn are present in the synthesis.

It is observed that on the 10% Sn/C the capacity is stable, after losses in the initial formation cycles, through 200 charge/discharge cycles. In general, a loss in capacity corresponds to a simultaneous sintering or mechanical pulverization of electrode through Sn volumetric changes. No capacity loss suggests no sintering after initial stabilization and that the SEI layer remains stable with little growth in thickness. We postulate that some of the Sn is initially not well anchored when deposited, and this fraction can sinter to form larger particles and increase SEI formation for the first few cycles. Indeed, there is a bimodal particle size distribution after charge/discharge testing. It is completely possible these large particles form in the first few cycles of testing. The majority of the Sn, in contrast, is in a particle form (~5 nm) which appears to be remarkably stable. This model explains the observed bimodal distribution as well as the observed electrode stability for this typically dynamic system.

The battery data can be shown to be consistent with a nearly 100% Sn 'effectiveness' model, that is very small and stable Sn particles. When the Sn capacity contribution is calculated by subtracting the activated carbon contribution, the value remains close to the 990 mAh g^{-1} theoretical capacity over 200 cycles (Fig. 6b). Indeed, after initial formation cycling stabilization during the first 20 cycles, the Sn capacity contribution decays only by 14% over the next 180 cycles, demonstrating the Sn nanoparticle stability induced by the RES synthesis. Additionally, the EIS study demonstrated that the well distributed, small Sn particles decreased the charge transfer resistance of the electrode, by augmenting conductive pathways for Li$^+$ and electrons, before and after SEI formation. This is consistent with strong bond formation between metal and carbon. Comparisons of these results with prior Sn/C composite literature in Table S1, demonstrates the augmented cycling stability obtained by this approach, even compared to composites with carbon encapsulated Sn nanoparticles. Future work could involve studying the impact of higher Sn loading content for the RES synthesis strategy, to determine if similar effectiveness and long-term stability is achieved, to produce high capacity anode materials.

It is worth considering the issue of 'size' at which particles can no longer be fully lithiated. Indeed, from the perspective of the users of supported metal catalysts, a similar morphology to Sn/C, the level of sintering observed would result in loss of ~one-half the active metal surface area, hence half the activity. This would not be acceptable for a catalyst. However; for anode use the issue is not surface area, rather it is bulk diffusion of ions, in and out of the Sn particle, or conduction of electrons from Sn to carbon support that eventually is impacted by Sn particle size. There is no evidence either was impacted by the growth observed, suggesting the Sn size at which there is an effective capacity loss is far larger than the maximum produced in this study.

Finally, the magnitude of the net capacity, carbon and Sn particles combined, should be considered relative to high quality graphite. In this regard it must be noted the capacity of all electrodes drops as discharge current increases. The best comparison point between the electrode in this study, and a commercial graphitic material, is for a full discharge in 7 h (C/7). The C7 capacity measured for this electrode, 340 mA/g, is about equal to that of the best commercial graphites. The frequently cited theoretical graphite capacity, ~370 mA/g, is only achieved for very slow discharges (C/12).

5. Conclusion

Evidence is presented to support the use of the Reduction Expansion Synthesis to generate high stability Sn/C anodes. An extra step aimed to activate the carbon support proved to be

indispensable to generate highly dispersed Sn particles able to survive the battery cycling test without disintegrating. The initial small particle size, despite a synthesis at 800 C, and the slow growth during nearly 200 test cycles, are consistent with the postulate that RES synthesis enables the formation of direct, strong bond between Sn and carbon substrate atoms. Direct evidence of a unique bond between Sn and support, very unusual in studies of supported metals, is found in the notably reduced interface resistance in the electrochemical data. This explanation is consistent with typical indirect evidence of enhanced bonding between particle and support. That is, strong metal-support bonding is the proposed explanation for minimal particles growth over many cycles, the apparent lack of any Sn electrode pulverization, and the absence of capacity fade due to expansion upon lithiation. Indeed, after 10 formation cycles, 94% of the capacity is retained during the next 190 lithiation cycles. Also notable is the very good net capacity of this novel electrode. To wit: the net capacity of the electrode, combined carbon (~280 mA/g) and Sn particles (nearly 1000 mA/g), closely matches the performance of the best graphites at a standard discharge current and rate (C/7). The research presented herein enhances our understanding of the Sn/C system and the metal/support interactions that will allow us to move a step ahead in the development of the next generation of energy storage devices.

Acknowledgements

Appendix A. Supplementary data

Supplementary data related to this article can be found at https://doi.org/10.1016/j.carbon.2018.02.079.

References

[1] Z.-S. Wu, G. Zhou, L.-C. Yin, W. Ren, F. Li, H.-M. Cheng, Graphene/metal oxide composite electrode materials for energy storage, Nano Energy 1 (2012) 107–131.

[2] G. Zhou, D.W. Wang, F. Li, L. Zhang, N. Li, Z.S. Wu, et al., Graphene-wrapped Fe_3O_4 anode material with improved reversible capacity and cyclic stability for lithium ion batteries, Chem. Mater. 22 (2010) 5306–5313.

[3] E.J. Yoo, J. Kim, E. Hosono, H.S. Zhou, T. Kudo, I. Honma, Large reversible Li storage of graphene nanosheet families for use in rechargeable lithium ion batteries, Nano Lett. 8 (2008) 2277–2282.

[4] A. Manthiram, A. Vadivel Murugan, A. Sarkar, T. Muraliganth, Nanostructured electrode materials for electrochemical energy storage and conversion, Energy Environ. Sci. 1 (2008) 621–638.

[5] M. Winter, J.O. Besenhard, Electrochemical lithiation of tin and tin-based intermetallics and composites, Electrochim. Acta 45 (1999) 31–50.

[6] S. Goriparti, E. Miele, F. De Angelis, E. Di Fabrizio, R. Proietti Zaccaria, C. Capiglia, Review on recent progress of nanostructured anode materials for Li-ion batteries, J. Power Sources 257 (2014) 421–443.

[7] I.A. Courtney, J.R. Dahn, Electrochemical and in situ x-ray diffraction studies of the reaction of lithium with tin oxide composites, J. Electrochem. Soc. 144 (1997) 2045–2052.

[8] J. Wang, F. Fan, Y. Liu, K.L. Jungjohann, S.W. Lee, S.X. Mao, et al., Structural evolution and pulverization of tin nanoparticles during lithiation-delithiation cycling, J. Electrochem. Soc. 161 (2014) F3019–F3024.

[9] S. Wakeland, Y. Cui, A. Knapp, M. Richard, J. Phillips, C. Luhrs, Multilayered nanoparticles generated by plasma methods for energy storage applications, Nanosci. Nanotech. Let. 4 (2012) 316–322.

[10] W.M. Zhang, J.S. Hu, Y.G. Guo, S.F. Zheng, L.S. Zhong, W.G. Song, et al., Tin-nanoparticles encapsulated in elastic hollow carbon spheres for high-

[11] K.T. Lee, Y.S. Jung, S.M. Oh, Synthesis of tin-encapsulated spherical hollow carbon for anode material in lithium secondary batteries, J. Am. Chem. Soc. 125 (2003) 5652–5653.

[12] G. Cui, Y.S. Hu, L. Zhi, D. Wu, I. Lieberwirth, J. Maier, et al., A one-step approach towards carbon-encapsulated hollow tin nanoparticles and their application in lithium batteries, Small 3 (2007) 2066–2069.

[13] X. Zhou, L. Yu, X.Y. Yu, X.W.D. Lou, Encapsulating Sn nanoparticles in amorphous carbon nanotubes for enhanced lithium storage properties, Adv. Energy. Mater. 6 (2016), 1601177.

[14] S. Wakeland, R. Martinez, J.K. Grey, C.C. Luhrs, Production of graphene from graphite oxide using urea as expansion-reduction agent, Carbon 48 (2010) 3463–3470.

[15] C. Luhrs, J. Phillips, Reductive Expansion Synthesis of Graphene, 2014. US Patent 8894886.

[16] L. Elbaz, J. Phillips, K. Artyushkova, K. More, E.L. Brosha, Evidence of high electrocatalytic activity of molybdenum carbide supported platinum nanorafts, J. Electrochem. Soc. 162 (2015) H681–H685.

[17] H. Zea, C.C. Luhrs, J. Phillips, Reductive/expansion synthesis of zero valent submicron and nanometal particles, J. Mater. Res. 26 (2011) 672–681.

[18] C. Luhrs, M. Kane, Z. Leseman, J. Phillips, Novel process for solid state reduction of metal oxides and hydroxides, Metall. Mater. Trans. B 44 (2013) 115–122.

[19] C.C. Luhrs, J. Phillips, H.R. Zea, Z. Leseman, Generation of Metal and Alloy Micron, Submicron or Nano Particles in Simple, Rapid Process, 2011. US Patent 8709126.

[20] H. Zea, C. Luhrs, J. Phillips, Production submicron and nano metallic particles via reductive/expansion method, Abstr. Pap. Am. Chem. Soc. 242 (2011).

[21] G. Antipas, Gas atomization of aluminium melts: comparison of analytical models, Metals 2 (2012) 202–210.

[22] H. Xu, N. Zou, Q. Li, Effect of ball milling time on microstructure and hardness of porous magnesium/carbon nanofiber composites, JOM 69 (2017) 1236–1243.

[23] J. Phillips, B. Xia, J.A. Menendez, Calorimetric study of oxygen adsorption on activated carbon, Themochimica Acta 312 (1998) 87–93.

[24] J.A. Menendez, B. Xia, J. Phillips, L.R. Radovic, On the modification and characterization of chemical surface properties of activated carbon: microcalorimetric, electrochemical, and thermal desorption probes, Langmuir 13 (1997) 3414–3421.

[25] J.A. Menéndez, J. Phillips, B. Xia, L.R. Radovic, On the modification and characterization of chemical surface properties of activated carbon: in the search of carbons with stable basic properties, Langmuir 12 (1996) 4404–4410.

[26] J. Phillips, D. Kelly, L. Radovic, F. Xie, Microcalorimetric study of the influence of surface chemistry on the adsorption of water by high surface area carbons, J. Phys. Chem. B 104 (2000) 8170–8176.

[27] A. Weibel, R. Bouchet, F. Boulc'h, P. Knauth, The big problem of small particles: a comparison of methods for determination of particle size in nanocrystalline anatase powders, Chem. Mater. 17 (2005) 2378–2385.

[28] X. Zhang, D.J. Gray, Y. Huot, Y. You, L. Bi, Comparison of optically derived particle size distributions: scattering over the full angular range versus diffraction at near forward angles, Appl. Opt. 51 (2012) 5085–5099.

[29] R.C. Woodward, J. Heeris, T.G. St Pierre, M. Saunders, E.P. Gilbert, M. Rutnakornpituk, et al., A comparison of methods for the measurement of the particle-size distribution of magnetic nanoparticles, J. Appl. Crystallogr. 40 (2007) s495–s500.

[30] M. Li, D. Wilkinson, K. Patchigolla, Comparison of particle size distributions measured using different techniques, Part. Sci. Technol. 23 (2005) 265–284.

[31] T. Lim, Fabrication of High Energy Density Sn/C Anodes Using Reduction Expansion Synthesis and Aerosol through Plasma Techniques, 2017. M.S.Thesis, Naval Postgraduate School.

[32] J. Phillips, B. Clausen, J.A. Dumesic, Iron pentacarbonyl decomposition over Grafoil. Production of small metallic iron particles, J. Phys. Chem. 84 (1980) 1814–1822.

[33] J. Phillips, J.A. Dumesic, Iron pentacarbonyl decomposition over grafoil: II. Effect of sample outgassing on decomposition kinetics, Appl. Surf. Sci. 7 (1981) 215–230.

[34] E. Hegenberger, N.L. Wu, J. Phillips, Evidence of strong interaction between iron particles and an activated carbon support, J. Phys. Chem. 91 (1987) 5067–5071.

[35] A.A. Chen, M.A. Vannice, J. Phillips, Effect of support pretreatments on carbon-supported Fe particles, J. Phys. Chem. 91 (1987) 6257–6269.

[36] J.M. Zhang, Z.L. Tan, C.J. Wang, J. Bi, W. Yi, Y. Sheng, et al., Effect of carbon support pretreatment on structure and performance of Pt/C electrocatalysts, Chin. J. Inorg. Chem. 31 (2015) 140–146.

[37] Y. Liu, N. Zhang, L. Jiao, Z. Tao, J. Chen, Ultrasmall Sn nanoparticles embedded in carbon as high-performance anode for sodium-ion batteries, Adv. Funct. Mater. 25 (2015) 214–220.